

X-ray magnetic circular dichroism and photoemission study of the diluted ferromagnetic semiconductor $\text{Zn}_{1-x}\text{Cr}_x\text{Te}$

Y. Ishida, M. Kobayashi, and J.I. Hwang

Department of Physics, University of Tokyo, Bunkyo-ku, Tokyo 113-0033, Japan

Y. Takeda, S.-i. Fujimori, T. Okane, K. Terai, Y. Saitoh, and Y. Muramatsu

Synchrotron Radiation Research Center, Japan Atomic Energy Agency, Sayo, Hyogo 679-5148, Japan

A. Fujimori

*Department of Physics, University of Tokyo, Bunkyo-ku, Tokyo 113-0033, Japan and
Synchrotron Radiation Research Center, Japan Atomic Energy Agency, Sayo, Hyogo 679-5148, Japan*

A. Tanaka

*Graduate School of Advanced Sciences of Matter,
Hiroshima University, Higashi-Hiroshima, Hiroshima 739-8530, Japan*

H. Saito and K. Ando

*Nanoelectronics Research Institute, National Institute of Advanced Industrial Science and Technology (AIST),
Tsukuba Central 2, Umezono 1-1-1, Tsukuba, Ibaraki 305-8568, Japan*

(Dated: February 2, 2008)

We have performed x-ray magnetic circular dichroism (XMCD) and valence-band photoemission studies of the diluted ferromagnetic semiconductor $\text{Zn}_{1-x}\text{Cr}_x\text{Te}$. XMCD signals due to ferromagnetism were observed at the Cr 2*p* absorption edge. Comparison with atomic multiplet calculations suggests that the magnetically active component of the Cr ion was divalent under the tetrahedral crystal field with tetragonal distortion along the crystalline *a*-, *b*-, and *c*-axes. In the valence-band spectra, spectral weight near the Fermi level was strongly suppressed, suggesting the importance of Jahn-Teller effect and the strong Coulomb interaction between the Cr 3*d* electrons.

Diluted magnetic semiconductors (DMSs) [1] showing high ferromagnetic Curie temperatures (T_C 's) are considered to be key materials for spintronics [2]. Ferromagnetism of II-VI-semiconductor-based DMS $\text{Zn}_{1-x}\text{Cr}_x\text{Te}$ thin films reported by Saito *et al.* [3, 4] has attracted much interest since the T_C was as high as 300 K and the large *sp-d* exchange constant, $N\beta$, was confirmed by magnetic circular dichroism (MCD) measurements in the visible to ultraviolet regions [5]. Subsequently, it was reported that control of ferromagnetism is possible through co-doping N or I during the thin film growth [6, 7, 8]. The ferromagnetism of $\text{Zn}_{1-x}\text{Cr}_x\text{Te}$ is qualitatively different from those of well-known III-V-semiconductor-based ferromagnetic DMSs such as $\text{Ga}_{1-x}\text{Mn}_x\text{As}$ and $\text{In}_{1-x}\text{Mn}_x\text{As}$: (1) The carrier concentration of $\text{Zn}_{1-x}\text{Cr}_x\text{Te}$ is as low as $\sim 10^{15} \text{ cm}^{-3}$ and the transport is semiconducting [3, 9], whereas ferromagnetism in $\text{Ga}_{1-x}\text{Mn}_x\text{As}$ and $\text{In}_{1-x}\text{Mn}_x\text{As}$ appears for high hole concentration ($\sim 10^{18}$ - 10^{20} cm^{-3}) and is most likely carrier induced [10]; (2) $N\beta$ of $\text{Zn}_{1-x}\text{Cr}_x\text{Te}$ is positive, that is, the hole spin created in the valence band tend to align in the same direction as the Cr 3*d* local spin, whereas those of $\text{Ga}_{1-x}\text{Mn}_x\text{As}$ and $\text{In}_{1-x}\text{Mn}_x\text{As}$ are negative [10, 11]. There have been several studies to understand the positive $N\beta$ in $\text{Zn}_{1-x}\text{Cr}_x\text{Te}$ from the electronic structure point of view [12, 13, 14, 15, 16, 17]. In this paper, we report on soft-x-ray MCD (XMCD) in Cr 2*p* core-level absorption and valence-band photoemission (PES) measurements to provide information about the

electronic structure of ferromagnetic $\text{Zn}_{1-x}\text{Cr}_x\text{Te}$ thin films. Detailed information such as the valence and crystal field of the magnetically active Cr site has been obtained since XMCD is an element-specific probe which is sensitive only to magnetically active component.

A 150-nm thick epitaxial thin film of $\text{Zn}_{1-x}\text{Cr}_x\text{Te}$ with $x=0.045$ ($T_C \sim 70 \text{ K}$) was grown on a 120-nm thick ZnTe layer on a 20-nm GaAs buffer layers prepared on a semi-insulating GaAs(001) substrate using the molecular beam epitaxy method as described elsewhere [3]. The sample surface was capped with a 3-nm thick ZnTe layer to avoid contamination for the $\text{Zn}_{1-x}\text{Cr}_x\text{Te}$ layer. Core-level absorption (XAS) spectra were recorded in the total-electron-yield mode at undulator beam line BL23SU of SPring-8 [18]. The degree of circular polarization was higher than 90 %. The monochromator resolution was $E/\Delta E > 10000$. Using a superconducting magnet, magnetic fields H up to 7 T were applied parallel and antiparallel to the propagation vector of the incident light and the sample surface. Photon helicity was switched at each photon energy. Valence-band PES measurements were performed at BL-18A of Photon Factory (PF), High Energy Accelerator Research Organization. An $x=0.043$ sample ($T_C \sim 70 \text{ K}$) without a capping layer and a ZnTe film as a reference were measured. The surface was cleaned by Ar-ion sputtering at 1.0 kV and subsequent annealing at 200°C. Cleanliness of the sample surface was checked by the absence of O 1*s* core-level PES signal. In order to avoid charging effects, the spec-

tra were taken at room temperature and at ~ 450 K. The base pressure was $\gtrsim 7.5 \times 10^{-10}$ Torr, and the resolution of the spectrometer (VG CLAM) including temperature broadening was ~ 200 meV.

Figure 1(a) shows the XAS and XMCD spectra taken at the Cr 2*p* absorption edge at $T=20$ K and $H=2$ T. Here, μ^+ and μ^- indicate absorption spectra for photon helicity parallel and antiparallel to the Cr 3*d* spin, respectively. The structures in the XAS spectra around $h\nu=576$ and 586 eV are due to absorption from the Cr 2*p*_{3/2} and Cr 2*p*_{1/2} core levels, respectively. The Cr 2*p* absorption overlaps with the tail of the broad absorption due to Te 3*d*→Te 5*p* transition. Since the Te 5*p* band is broad and structureless, we assumed a polynomial background to separate the Te 3*d* absorption from Cr 2*p* absorption, as shown by dashed curves in Fig. 1(a). The XAS and XMCD spectra at the Cr 2*p* edge show multiplet structures, which are fingerprints of the localized nature of the Cr 3*d* electrons in a crystal field.

Following the orbital sum rule [19], the energy integral of the XMCD signal in the entire region of the Cr 2*p* absorption is proportional to the orbital moment of the Cr 3*d* electrons, $\langle L_z \rangle$. If the Cr ions are isovalently substituting Zn and become Cr²⁺ (3*d*⁴) under a crystal field of T_d symmetry as shown in the left panel of Fig. 1(b), $\langle L_z \rangle$ becomes negative or the integrated XMCD becomes positive since the filling of the 3*d* orbital is less than half and there is orbital degrees of freedom in the t_2 states. However, as shown in Fig. 1(a), the integral became very small or slightly negative, indicating that $\langle L_z \rangle$ is largely quenched compared with the value of the Cr²⁺ ion in the T_d -symmetry crystal field. In fact, Vallin and co-workers have shown in their optical absorption study that dilute Cr²⁺ ions in bulk ZnTe are subject to Jahn-Teller distortion [20, 21] as shown in the right panel of Fig. 1(b), leading to the lift of the orbital degeneracy and the quenching of $\langle L_z \rangle$.

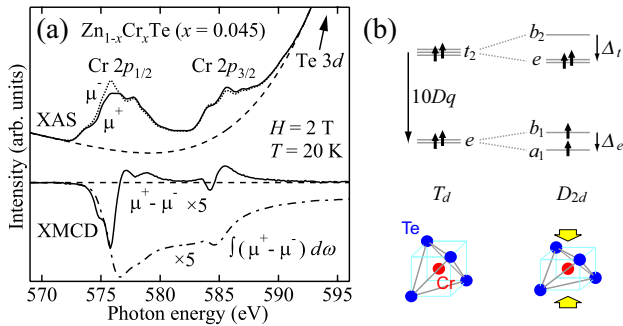


FIG. 1: Cr 2*p* XAS and XMCD spectra (a) Experimental XAS and XMCD spectra. The dashed curve is a polynomial fit to the tail of the broad Te 3*d* absorption. The dot-dashed curve shows the energy integral of the XMCD. (b) Single-electron energy levels in a T_d (left) and in a D_{2d} symmetry (right). The t_2 (e) states under the T_d symmetry are split into b_2 and e (b_1 and a_1) under the D_{2d} symmetry.

Figure 2(a) shows H dependence of XMCD at the Cr

2*p* absorption edge. The strength of XMCD increased with increasing H . We could observe dichroism down to $H \sim 0.1$ T as shown in panels (a) and (b), indicating the presence of substantial residual magnetization of the Cr 3*d* electrons. The convex behavior of the XMCD strength above $H=2$ T [panel (b)] suggests that there were Cr ions showing superparamagnetism [8] as well as paramagnetism in the present sample. In the inset of Fig. 2(a), we show XMCD spectra around the Cr 2*p*_{3/2} peak normalized to the XMCD peak intensity. The normalized XMCD spectra overlap with each other except for a dip structure around $h\nu \sim 578$ eV which is discussed later. This indicates that there were a single chemical environment for the magnetically active Cr ions in Zn_{1-x}Cr_xTe. This is in line with the unchanged line shapes of the visible to ultraviolet MCD under varying magnetic field [3, 22].

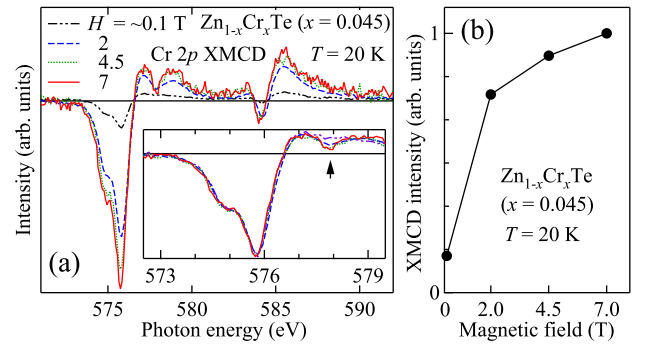


FIG. 2: (Color online) Magnetic-field dependence of XMCD in the Cr 2*p* absorption of Zn_{1-x}Cr_xTe ($x=0.045$). (a) XMCD at various H taken at $T=20$ K. Inset shows the normalized XMCD. (b) Intensity of Cr 2*p* XMCD at $T=20$ K as a function of H .

In Fig. 3, we compare the XAS and XMCD spectra with those calculated using atomic multiplet theory taking into account the Jahn-Teller distortion. The calculated spectra for T_d and D_{2d} symmetries with high-spin configurations are shown in Fig. 3(b) and (c), respectively. The crystal-field parameters for D_{2d} symmetry, namely, $10Dq=-0.55$ eV and $\Delta_t=-0.20$ eV, and $\Delta_e=-0.10$ eV have been adopted from Ref. [20]. In the calculation of the spectra under D_{2d} symmetry, we have assumed that there are equal numbers of tetragonally-distorted Cr sites along the a , b and c axes because the film was relaxed because of the large mismatch in the lattice constant ($a=6.10$ Å for ZnTe and $a=5.65$ Å for GaAs) and free from the epitaxial strain from the substrate [22]. In Fig. 3, we have also indicated $\langle L_z \rangle$. The experimental $\langle L_z \rangle$ has been calculated using the orbital sum rule [19]. One can see the suppressed $\langle L_z \rangle$ in the case of D_{2d} compared to the case of T_d , which is in accord with the observed suppression of the Cr 3*d* orbital moment (Fig. 1). Furthermore, the XMCD lineshape is well reproduced in the calculated spectra for the D_{2d} symmetry compared to that for the T_d symmetry particularly in the Cr 2*p*_{3/2}

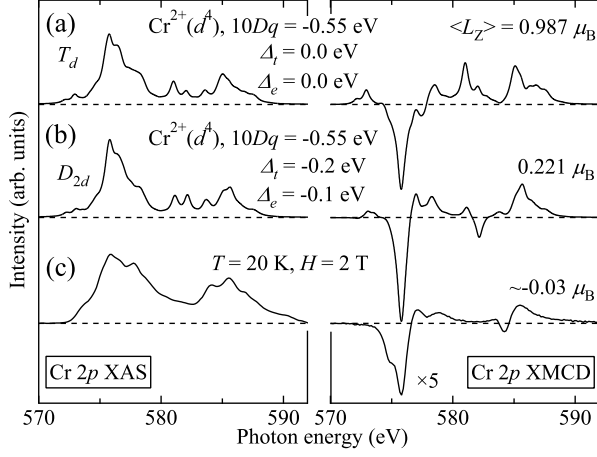


FIG. 3: Cr 2p XAS and XMCD spectra calculated using atomic multiplet theory for $\text{Cr}^{2+} (d^4)$ in the T_d -symmetry crystal field (a), in the D_{2d} -symmetry crystal field (b; see, text), and the experimental spectra (c). Background-subtracted $(\mu^+ + \mu^-)/2$ has been adopted for the experimental XAS spectrum. The orbital moment per Cr ion in the ground state is also indicated for each panel.

absorption region. The XAS lineshape is also well reproduced for the D_{2d} symmetry except for a peak around 578 eV, which may originate from a small amount of other Cr compound(s). In fact, XMCD around 578 eV showed a H dependence different from the other XMCD features, as described above. Thus, we conclude that the experimental spectra are well reproduced if the Jahn-Teller effect is included. The lift of the orbital degeneracy due to Jahn-Teller effect will directly affect the sp - d exchange interaction as studied theoretically in Refs. [17, 23, 24].

The observed strength of XMCD at the Cr 2p absorption edge was $\sim 20\%$ ($\sim 0.4 \mu_B$ per Cr ion) of the theoretical value where the spin is fully polarized [Note that, in Fig. 3(b) and (c), the experimental dichroism is multiplied by a factor of 5.] This value is somewhat smaller than that derived from the magnetization measurements, for example, $2.2 \pm 0.3 \mu_B$ reported for $x=0.035$ sample [22]. It is possible that there is a magnetically dead layer near the surface region, and some portion of the Cr ion contributes either to paramagnetism or to antiferromagnetism.

Finally, we show the valence-band PES spectra of $\text{Zn}_{1-x}\text{Cr}_x\text{Te}$ ($x=0.043$) and ZnTe thin films in Fig. 4. At the excitation energy of $h\nu=48\text{ eV}$, the atomic photoionization cross-section of Cr 3d is ~ 20 times larger than that of Te 5p [26]. In fact, the intensity of the valence band of Cr-doped ZnTe is ~ 2 times higher than the valence-band intensity of ZnTe mainly composed of Te 5p states as shown in the top panel of Fig. 4. By subtracting the spectrum of ZnTe from that of $\text{Zn}_{1-x}\text{Cr}_x\text{Te}$ ($x=0.043$), we have deduced the Cr 3d partial density of states (PDOS) as shown in the middle panel of Fig. 4. For comparison, we show the calculated total density of states

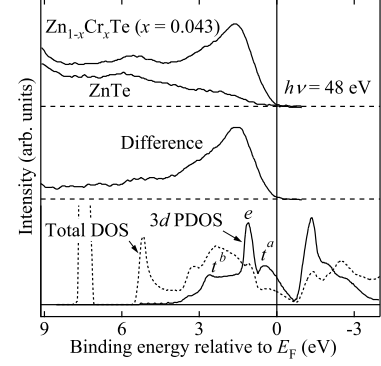


FIG. 4: Valence-band PES spectra of $\text{Zn}_{1-x}\text{Cr}_x\text{Te}$ ($x=0.043$) and ZnTe and their difference spectra. The theoretical total density of states (DOS) and Cr 3d partial DOS (PDOS) are taken from Ref. [25].

(DOS) and the Cr 3d PDOS of $\text{Zn}_{1-x}\text{Cr}_x\text{Te}$ ($x=0.25$) calculated within the local-spin-density-function approximation [25] in the bottom panel of Fig. 4. One can see a peak at ~ 1.5 eV and a broad shoulder centered at ~ 3 eV in the experimental Cr 3d PDOS, which can be assigned to nonbonding Cr e and bonding Cr t_2 states, and thus agreement between experiment and theory is good on the high binding energy side of the valence band. On the other hand, the spectral weight near the Fermi level was strongly suppressed in the experimental spectra compared to the theoretical Cr 3d PDOS which shows half-metallic behavior [25]. This discrepancy may be due to the small Cr concentration of $x=0.043$ in the present study, which was not enough for an impurity band to form, or because the experiment was performed at room temperature in the paramagnetic phase. Since the transport properties of $\text{Zn}_{1-x}\text{Cr}_x\text{Te}$ are p -type semiconducting [9] even at high doping levels of $x \sim 0.20$ [3], we believe that the suppression of the spectral weight at the Fermi level is common to the ferromagnetic $\text{Zn}_{1-x}\text{Cr}_x\text{Te}$. If the tetragonal distortion splits the Cr 3d t_2 orbitals in the T_d symmetry as suggested from the XMCD study, a gap will open in the Cr 3d t_2 impurity band which may explain the suppressed spectral weight around the Fermi level. A strong Coulomb interaction between Cr 3d electrons will also suppress the spectral weight at the Fermi level. Therefore, it is important to include the distortion effect as well as the strong Coulomb interaction effect to understand the ferromagnetic $\text{Zn}_{1-x}\text{Cr}_x\text{Te}$.

In summary, we have confirmed the Cr 3d origin of the ferromagnetism in $\text{Zn}_{1-x}\text{Cr}_x\text{Te}$ ($x=0.045$) thin film by XMCD measurements. Comparison with atomic multiplet calculation indicated that the Cr ion is divalent and substituting the Zn site of the host ZnTe and that the Cr ions were subject to tetragonal distortion due to Jahn-Teller effect as observed in bulk $\text{Zn}_{1-x}\text{Cr}_x\text{Te}$ [20, 21]. The suppressed spectral weight near the Fermi level in the valence-band spectra was discussed in terms of the distortion effect and the strong Coulomb effect between

Cr $3d$ electrons.

We thank T. Okuda, A. Harasawa, and T. Kinoshita for help during the experiment at PF, and T. Mizokawa for useful discussion and comments. This work was supported by a Grant-in-Aid for Scientific Research in Pri-

ority Area “Semiconductor Nanospintronics” (14076209) from MEXT, Japan. The experiment at PF was approved by the Photon Factory Program Advisory Committee (Proposal No. 04G002).

-
- [1] J. K. Furdyna, J. Appl. Phys. **64**, R29 (1988).
 - [2] I. Žutić, J. Fabian, and S. D. Sarma, Rev. Mod. Phys. **76**, 323 (2004).
 - [3] H. Saito, V. Zayets, S. Yamagata, and K. Ando, Phys. Rev. Lett. **90**, 207202 (2003).
 - [4] H. Saito, V. Zayets, S. Yamagata, and K. Ando, J. Appl. Phys. **93**, 6796 (2003).
 - [5] K. Ando, Science **312**, 1883 (2006).
 - [6] N. Ozaki, I. Okabayashi, T. Kumekawa, N. Nishizawa, S. Marcet, S. Kuroda, and K. Takita, Appl. Phys. Lett. **87**, 192116 (2005).
 - [7] N. Ozaki, I. Okabayashi, T. Kumekawa, N. Nishizawa, S. Marcet, S. Kuroda, and K. Takita, Phys. Rev. Lett. **97**, 037201 (2006).
 - [8] S. Kuroda, N. Nishizawa, K. Takita, M. Mitome, Y. Bando, K. Osuch, and T. Dietl, Nature Mat. **6**, 440 (2007).
 - [9] H. Saito, W. Zayets, S. Yamagata, and K. Ando, J. Appl. Phys. **91**, 8085 (2002).
 - [10] H. Ohno, J. Magn. Magn. Mat. **200**, 110 (1999).
 - [11] K. Ando, in *Magneto-Optics* **69**, edited by S. Sugano and N. Kojima, Springer Series in Solid (Springer, Berlin, 2000).
 - [12] W. Mac, N. T. Khoi, A. Twardowski, J. A. Gaj, and M. Demianiuk, Phys. Rev. Lett. **71**, 2327 (1993).
 - [13] W. Mac, A. Twardowski, and M. Demianiuk, Phys. Rev. B **54**, 5528 (1996).
 - [14] A. K. Bhattacharjee, Phys. Rev. B **46**, 5266 (1992).
 - [15] J. Blinowski and P. Kacman, Phys. Rev. B **46**, 12298 (1992).
 - [16] A. K. Bhattacharjee, Phys. Rev. B **49**, 13987 (1994).
 - [17] T. Mizokawa and A. Fujimori, Phys. Rev. B **56**, 6669 (1997).
 - [18] J. Okamoto, K. Mamiya, S.-I. Fujimori, T. Okane, Y. Saitoh, Y. Muramatsu, A. Fujimori, S. Ishiwata, and M. Takano, AIP Conf. Proc. **705**, 1110 (2004).
 - [19] B. T. Thole, P. Carra, F. Sette, and G. van der Laan, Phys. Rev. Lett. **68**, 1943 (1992).
 - [20] J. T. Vallin, G. A. Slack, S. Roberts, and A. E. Hughes, Phys. Rev. B **2**, 4313 (1970).
 - [21] J. T. Vallin and G. D. Watkins, Phys. Rev. B **9**, 2051 (1974).
 - [22] H. Saito, V. Zayets, S. Yamagata, and K. Ando, Phys. Rev. B **66**, 081201R (2002).
 - [23] A. K. Bhattacharjee, Phys. Rev. B **49**, 13987 (1994).
 - [24] W. Mac, A. Twardowski, and M. Demianiuk, Phys. Rev. B **54**, 5528 (1996).
 - [25] T. Fukushima, K. Sato, H. Yoshida, and P. H. Dederichs, Jpn. J. Appl. Phys. (2004).
 - [26] I. Lindau, Atomic Data Nucl. Data Tables **32**, 1 (1985).